JGR Solid Earth

RESEARCH ARTICLE
10.1029/2019JB018558

Key Points:
- Most earthquakes in the Delaware Basin since 2009 are likely induced by wastewater disposal, with ~5% induced by hydraulic fracturing
- ~37,000 earthquakes with $M_W \leq 3.4$ were identified with regional and local template matching
- Geologic structures may act as low-permeability boundaries that influence the occurrence and location of induced seismicity

Supporting Information:
- Data S1
- Table S1
- Table S2
- Table S3

Correspondence to:
R. J. Skoumal,
rskoumal@usgs.gov

Citation:
Skoumal, R. J., Barbour, A. J., Brudzinski, M. R., Langenkamp, T., & Kaven, J. O. (2020). Induced seismicity in the Delaware Basin, Texas. *Journal of Geophysical Research: Solid Earth*, *125*, e2019JB018558. https://doi.org/10.1029/2019JB018558

Received 20 AUG 2019
Accepted 13 DEC 2019
Accepted article online 14 DEC 2019

Induced Seismicity in the Delaware Basin, Texas

Robert J. Skoumal[1], Andrew J. Barbour[1], Michael R. Brudzinski[2], Teresa Langenkamp[2], and J. Ole Kaven[1]

[1]Earthquake Science Center, U.S. Geological Survey, Menlo Park, CA, USA, [2]Department of Geology and Environmental Earth Science, Miami University, Oxford, OH, USA

Abstract The seismicity rate in the Delaware Basin, located in western Texas and southeastern New Mexico, has increased by orders of magnitude within the past ~5 years. While no seismicity was reported in the southern Delaware Basin during 1980–2014, 37 earthquakes with M > 3 occurred in this area during 2015–2018. We generated an improved catalog of ~37,000 earthquakes in this region during 2009–2018 by applying multistation template matching at both regional and local stations using all earthquakes in the Advanced National Seismic System (ANSS) and TexNet catalogs. We found that the vast majority of the seismicity is most likely associated with wastewater disposal, while at least ~5% of the seismicity was induced directly by hydraulic fracturing. We inferred far-field effects of wastewater disposal inducing earthquakes over distances >25 km. The spatial limits of seismicity correlate with geologic structures that include the Central Platform and Grisham Fault, suggesting hydrologic compartmentalization by low-permeability boundaries. Given that the seismicity rate increased throughout the duration of the study, if industry operations continue unaltered, it is likely that both the seismicity rate and number of M > 3 earthquakes may continue to increase in the future.

1. Introduction

The seismicity rate in the central and eastern United States (CEUS) increased forty-fold within the past decade predominantly as a result of human activities (Ellsworth, 2013; van der Baan & Calixto, 2017). This recent increase in seismicity rate in the CEUS has largely been attributed to large-volume wastewater disposal (WD) wells injecting fluids into deep sedimentary formations (e.g., Keranen et al., 2014; Rubinstein & Mahani, 2015). Other human activities, including hydraulic fracturing (HF; e.g., Skoumal et al., 2015b) and carbon sequestration (e.g., Kaven et al., 2015), have induced seismicity to a lesser extent in the CEUS.

Texas has a long history of induced seismicity with earthquakes attributed to human activities, dating back to at least the 1920s (Frohlich et al., 2016). Over the past century, earthquakes have been associated with WD, waterflooding, injection of supercritical CO_2, and hydrocarbon production in the state (e.g., Frohlich et al., 2016). Numerous cases of induced seismicity have also been recently identified in Texas, namely, the Azle (Hornbach et al., 2015), Dallas-Fort Worth (Frohlich et al., 2011), and Timpson (Frohlich et al., 2014) earthquake sequences. Although HF-induced seismicity is pervasive in the neighboring state of Oklahoma (Skoumal, Ries, et al., 2018), no HF-induced seismicity has been previously reported in Texas with the exception of some potential cases in the Texas panhandle (Walter et al., 2018).

The Permian Basin is a broad sedimentary basin located in western Texas and southeastern New Mexico (Figure 1). Hydrocarbons have been produced from the Basin since the 1930s, with the majority of earthquakes since then suggested to be induced (Frohlich et al., 2016). These induced earthquakes include events near the town of Snyder that were associated with waterflooding during 1974–1982 (Davis & Pennington, 1989) and injection of supercritical CO_2 during 2006–2011 (Gan & Frohlich, 2013).

In the 1970s, enhanced recovery and hydrocarbon production were associated with cases of induced seismicity in the Delaware Basin (e.g., Doser et al., 1991), a subbasin located in the western Permian Basin (Figure 1). In the northwestern extent of the Delaware Basin, induced seismicity was associated with WD in the Dagger Draw oil field beginning in the late 1990s (Herzog, 2014; Zhang et al., 2016). During 1970–2014, the Advanced National Seismic System (ANSS) comprehensive catalog (ComCat) contains 20 $M \geq 3$ earthquakes in the Delaware Basin, 14 of which were associated with the Dagger Draw oil field. During 2015–2018, there were 24 $M \geq 3$ earthquakes in the Delaware Basin. Even with the long-lived Dagger Draw-induced sequence considered, this recent seismicity represents an order of magnitude

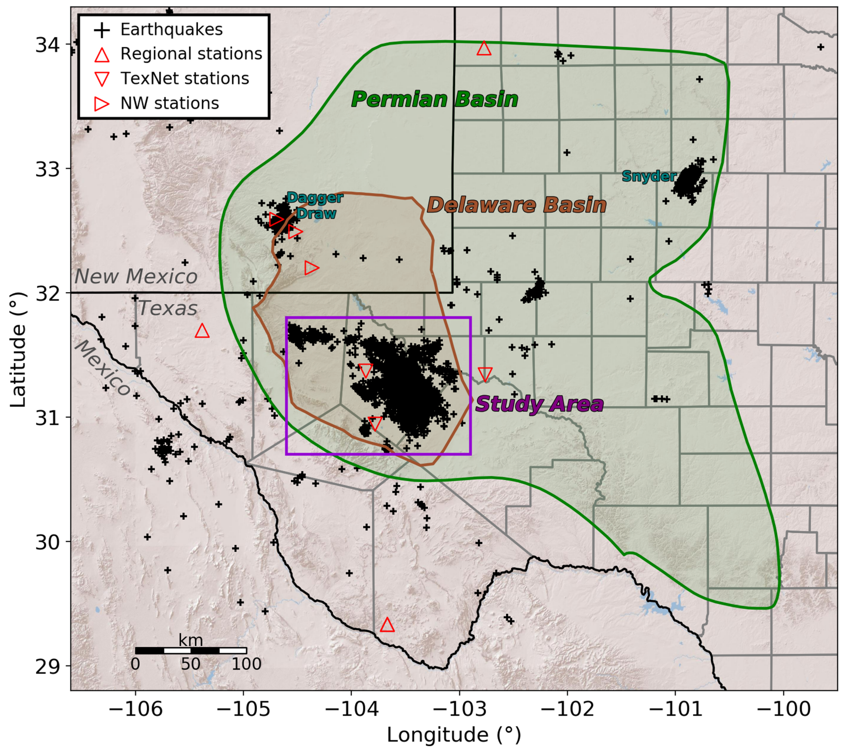

Figure 1. Map of seismicity near the Permian Basin (green polygon) in western Texas and southeastern New Mexico, including the Dagger Draw (Herzog, 2014; Zhang et al., 2016) and Snyder (Davis & Pennington, 1989; Gan & Frohlich, 2013) sequences. Epicenters (black crosses) are from the Advanced National Seismic System (ANSS) catalog, New Mexico (Pursley et al., 2013), and TexNet earthquake catalogs. Our study area (purple rectangle) is located primarily within the Delaware Basin (brown polygon). Triangles denote seismometers used in the three template matching applications.

increase in the earthquake rate. The only earthquake listed in ComCat in our study area (Figure 1) before 2009 was a M_b 4.8 earthquake (on 1 August 1975) and was found to be a naturally occurring, tectonic event (Frohlich et al., 2016).

This study principally seeks to better characterize the seismicity that has occurred in the Delaware Basin over the past decade, identify the causes of the earthquakes, offer explanations for why earthquakes are induced in some regions of the Basin but not others, and document the far-field effects of industrial operations in the area.

2. Materials and Methods

2.1. Template Matching

Template matching is an important technique for the characterization of repetitive seismic sources (e.g., Schaff & Waldhauser, 2010). As induced seismicity commonly occurs as swarms containing similar, repeating events, template matching aids our understanding of induced earthquakes by detecting smaller magnitude earthquakes that are generally missed in routine processing (e.g., Skoumal et al., 2015a). We implemented three template matching approaches using different combinations of stations and cataloged earthquakes, with each application being tailored to address differing motivations. These motivations are (1) increasing the number of detected earthquakes over the past decade using a regional network, (2) detecting recent seismicity in the past few years using a more local set of a stations, and (3) detecting the onset of seismicity in the northwestern corner of our study area to investigate potential far-field effects of industrial operations.

Our general approach is as follows. Continuous seismic data used in template matching are bandpass filtered between 5 and 15 Hz. Template waveforms are 20 s in length and begin 5 s before the P-phase arrival on vertical channels and 5 s before the S-phase arrival on horizontal channels. As it is not practical to manually inspect all newly detected events, we use a conservative detection threshold of 15 times the median absolute deviation (MAD) of the hourly network normalized cross-correlation coefficients (NNCCC) to identify new earthquakes. Detected events must also exceed a NNCCC of 0.25. These template matching parameters are similar to those that have been previously utilized to study induced seismicity in a variety of different regions in North America (e.g., Skoumal et al., 2014). Newly detected earthquakes ("detection(s)") are assigned the hypocenter location of the catalog ("template") earthquake that produces the highest NNCCC: MAD coefficient.

The first template matching we perform is on 126 ANSS ComCat earthquakes in our study area that occurred between 1 January 2009 and 31 December 2018 using four regional stations located in western Texas (Figure 1): US.MNTX, TA.MSTX, IM.TX31, and IM.TX32. The primary objective of this template matched catalog was to better characterize the early onset of induced seismicity, and these stations have the most reliable uptime during this decade-long study window.

The second template matching we perform is on the 3,712 earthquakes from the TexNet earthquake catalog between 28 March 2017 and 31 December 2018 using three seismometers that were located in the Delaware Basin area (Figure 1): TX.MNHN, TX.PB01, and TX.PECS. The objective of this catalog is to characterize the recent earthquake activity using a set of local seismometers. Data are not available at all three of these stations until 13 October 2017, and only one station was utilized in the detections for the preceding 6 months. In this case, due to the increased potential for false positives owing to local cultural noise on a single station, a detected event must also exceed a NNCCC of 0.5 in addition to the previously described 15×MAD threshold.

The third and final template matching we perform is on the 319 earthquakes in the TexNet catalog in the northwestern portion of our study area between 29 February 2016 and 31 December 2018. We use three seismometers located in New Mexico, ~70 km north of the earthquakes (Figure 1): SC.DAG, SC.GDL2, and SC.SRH. The motivation for this processing is to extend the earthquake detection back to 2016 to better characterize the temporal onset of seismicity and investigate possible far-field effects of fluid injection.

Following the approach of Schaff and Richards (2014), we estimate earthquake magnitudes for our three template matched catalogs by comparing the unnormalized correlation coefficients between the newly detected events and its respective template earthquake. The relative magnitude estimate is given as

$$\delta_{\mathrm{mag}} = \log_{10}[\max(\boldsymbol{x}\star\boldsymbol{y})/(\boldsymbol{x}\cdot\boldsymbol{x})] \tag{1}$$

where ★ represents cross correlation, centered dot (·) is the dot product, and $\boldsymbol{x}$ and $\boldsymbol{y}$ represent the waveforms of the template and detected earthquake, respectively. The δ_{mag} value is determined for all channels that are used to detect a given detected event, and the median of the δ_{mag} values is used to assign a magnitude to the newly detect event.

We estimate the magnitude of completeness (M_C) for the ANSS and TexNet catalogs by applying the maximum curvature algorithm (Wiemer & Wyss, 2000) to 1,000 samplings of our catalog with each sampling containing 90% of the dataset. The mean of these values added to a magnitude correction of 0.2 is used as the M_C for a given catalog. This completeness is then used with the maximum likelihood estimation to determine the Gutenberg-Richter b-values. As with the M_C calculation, the b-value is also estimated using the mean of 1,000 bootstrap iterations.

While template matching is a powerful tool for detecting small magnitude events that would otherwise be missed, the technique can only identify earthquakes with waveforms similar in character (i.e., similar location and mechanism) to those in the original catalog. Cross-correlation coefficients decrease precipitously as interevent distances exceed 1 km (Schaff & Waldhauser, 2005), so newly detected events are limited to those in near template events. For this reason, the true M_C for a large region cannot be lower than the original catalog even though the number of detected earthquakes is often increased by roughly an order of magnitude. The quality of the template matched catalog will depend on how robustly the template waveforms represent the lower-magnitude seismicity in the area of interest.

2.2. Wastewater Disposal Records

We obtain all reported WD data from the Texas Railroad Commission website and select the 2,836 WD wells located around our study region (Figure 2). Disposal volume availability begins in January 2007 and is

10.1029/2019JB018558

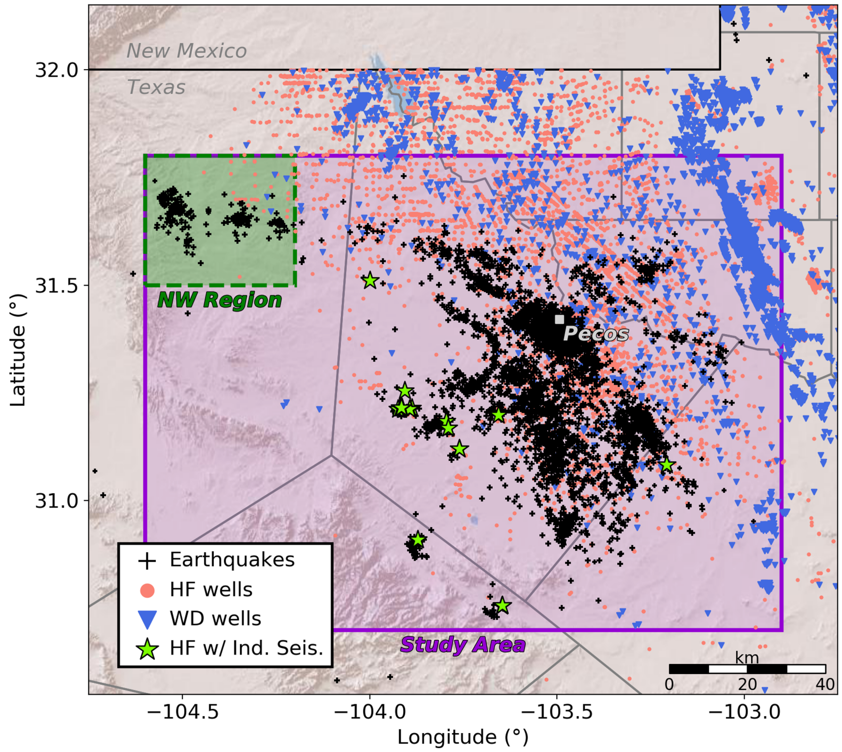

Figure 2. Map of the earthquakes (black crosses), hydraulic fracturing (HF) wells (red circles), and wastewater disposal (WD) wells (blue triangles) in Texas around our selected study region (purple rectangle). Wells in New Mexico are not shown. The northwestern region (green rectangle) where we investigate far field effects is also shown. The areas with the most prominent cases of HF-induced seismicity are represented by green stars. The city of Pecos, Texas, is represented with a square.

reported in monthly increments (Figure 3a). As the reporting completeness varies between wells in 2018, we only consider the disposal volumes from January 2007 through December 2017. In this time period, a total of ~7.0×10^8 m^3 (4.4×10^9 bbl) of wastewater was injected, with ~40% injected in 2016–2017 (Figure 3a). We use the permitted disposal depths for the wells as an estimate for the true vertical depth of the injection interval.

2.3. HF Records

We obtained all available information on the timing and location of HF stimulations from FracFocus, a national registry used to document chemicals used in hydraulic stimulations. While the investigation of HF-induced seismicity is not the intended purpose of FracFocus, this is the only publicly available source that includes an approximate spatiotemporal record of HF stimulations in Texas. Reported operational times are in the form of an approximate start and end date of stimulation activities at a well, with no information regarding the number, timing, or duration of individual stimulation stages disclosed. In total, there were 4,986 HF wells reported in the Texas portion of the Delaware Basin between 5 January 2011 and 31 December 2018.

In Oklahoma, regulations mandate the reporting to FracFocus, but records occasionally have missing or incomplete data, and ~8% of stimulated wells are not reported (Skoumal, Ries, et al., 2018). Similar regulations in Texas that require the reporting to FracFocus were implemented on 1 February 2012, but the true completeness of FracFocus reporting in Texas after this date is unknown. Although it is incomplete, information from 168 wells in Texas were voluntarily reported to FracFocus before 1 February 2012. In cases where we identified HF-induced seismicity, well data were obtained from the Texas Railroad Commission to ensure well metadata are consistent with records in FracFocus. We assume all other reporting to be accurate for the purposes of this study.

10.1029/2019JB018558

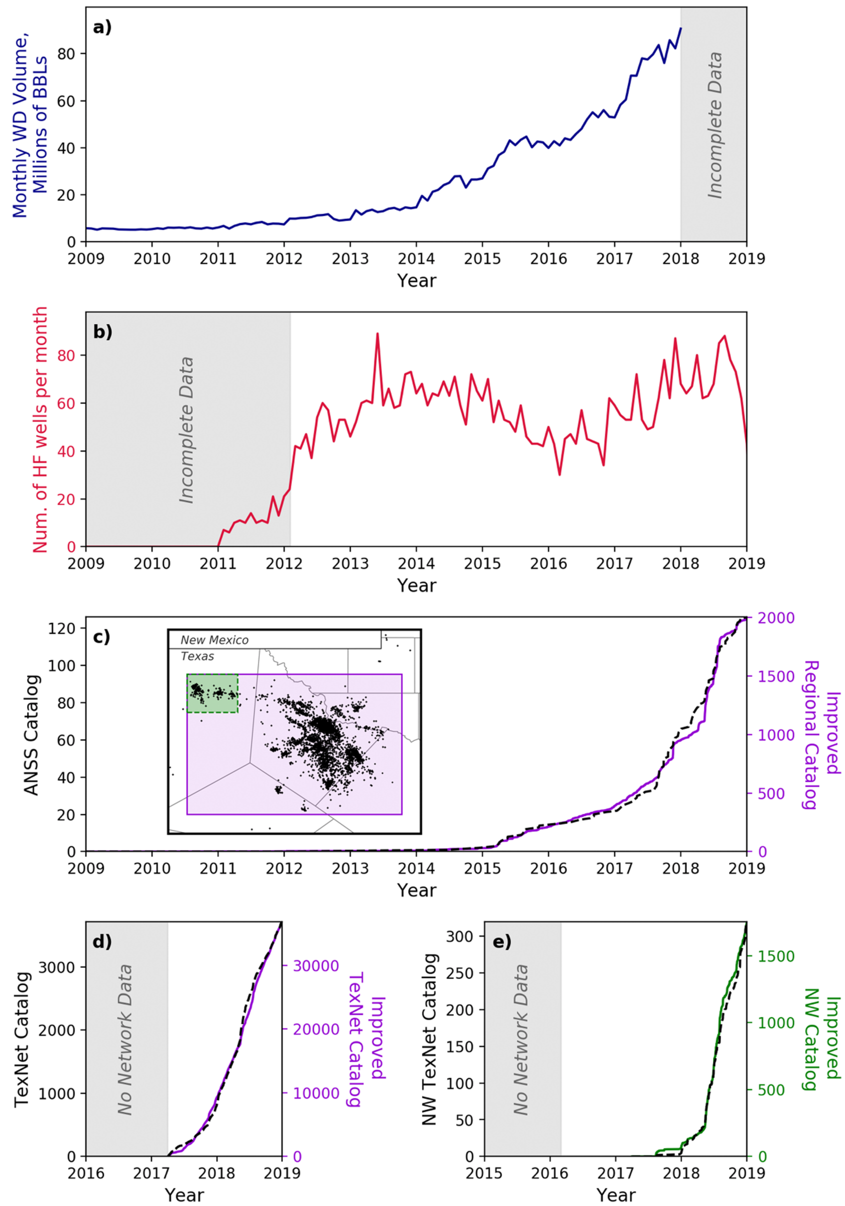

Figure 3. Industrial activities and earthquake counts in our study area of the Delaware Basin (Figure 1). (a) Monthly injection volumes for wastewater disposal (WD) wells. (b) Number of hydraulic fracturing (HF) wells that began stimulating per month. (c) Cumulative number of Advanced National Seismic System (ANSS) catalog earthquakes (dashed black line) compared with the number of earthquakes detected by applying regional template matching to the ANSS catalog (purple line) during 2009–2018. (d) Cumulative number of TexNet catalog earthquakes (black dashed line) compared with the number of earthquakes detected by applying local template matching to the TexNet catalog between 29 March 2017 and 31 December 2018 (purple line). (e) Cumulative number of TexNet cataloged earthquakes in the northwestern portion of the study area (Figure 2) compared with the number of earthquakes by applying template matching using seismometers in southern New Mexico. The improved regional and improved TexNet catalogs in (c) and (d) (purple lines) correspond to earthquakes within the purple rectangle in the inset of (c). The improved NW catalog in (e) (green line) corresponds to the green rectangle in the inset of (c).

2.4. Identifying Hydraulic Fracturing-Induced Seismicity With ΔEQ_{rate}

Due to the large number of detected earthquakes and reported HF wells, we use a modified approach of Skoumal, Ries, et al. (2018) to identify cases of HF-induced seismicity. Previously, Skoumal, Ries, et al. (2018) flagged cases of HF-induced seismicity in Oklahoma by identifying changes in seismicity rate ($\Delta EQ_{T,D}$) that coincided with timings of HF wells given a set of user-defined time and distance windows.

With that method, it was assumed that if HF induced earthquakes, the seismicity rate near the well would be higher during the stimulation than in periods before and after the stimulation. The approach was defined as

$$\Delta \mathrm{EQ}_{T,D} = \frac{1}{|T| \times |D|} \sum_{t \in T} \sum_{d \in D} \frac{2 \times \mathrm{EQ}_{0,d}}{\mathrm{EQ}_{-t,d} + \mathrm{EQ}_{+t,d}} \tag{2}$$

where $T = \{5,15,30\}$ days, $D = \{5,7.5,10\}$ km, and $\mathrm{EQ}_{\pm t,d}$ represents the number of earthquakes per day within time window t and distance d from a given well. While this method was found to significantly aid the classification of HF-induced seismicity in Oklahoma (Skoumal, Ries, et al., 2018), this implementation has a number of limitations. First, the time and distance thresholds (T, D) that are selected can have a significant influence over the results. While multiple distance thresholds were used to give an intrinsic weighting to earthquakes in close proximity to a HF well, the earthquakes up to a given distance threshold d were weighted the same. Second, while the largest seismicity rate would be expected to occur during the stimulation for induced sequences, HF-induced seismicity can cause aftershocks with decaying magnitudes in the days to months following the stimulation (e.g., Skoumal et al., 2015a). Hence, if induced aftershocks occur following the completion of a stimulation, they would negatively impact the proper classification. Third, HF wells that induce earthquakes often cluster spatially; if the conditions in a given area are suitable for induced seismicity, HF wells in that area would have an increased likelihood of inducing earthquakes (Skoumal et al., 2016; 2018). If the HF wells are in close proximity to each other and stimulated at similar times, induced earthquakes caused by a given well would negatively influence the detection at the other well(s).

Here, we use a modified approach addressing the limitations of Skoumal, Ries, et al. (2018) to flag cases of HF-induced seismicity defined as

$$\Delta \mathrm{EQ}_{\mathrm{rate}} = \frac{2 \times \sum \left(d - \boldsymbol{D}_{0,d}\right)}{\sum \left(d - \boldsymbol{D}_{-t,d}\right) + \sum \left[\left(d - \boldsymbol{D}_{+t,d}\right) \times \left(\boldsymbol{T}_{+t,d}\right)\right]} \tag{3}$$

where d is a distance constant, $\boldsymbol{D}_{\pm t,d}$ represents the distances of earthquakes within time window t and distance d from a given HF well, and $\boldsymbol{T}_{+t,d}$ represents the number of days an earthquake occurred following a stimulation within time window t and distance d from a given HF well. The calculations of $\boldsymbol{D}_{\pm t,d}$ and $\boldsymbol{T}_{+t,d}$ excluded any earthquakes that occurred during the time of other HF stimulations within distance d. Here, we use d=7 km, and t=30 days. The distance d of 7 km was selected as it was a conservative sum of (1) the estimate of the 99th percentile of reported horizontal location errors in the TexNet catalog (~4 km), (2) the assumed distance that a horizontal lateral extends beyond the well pad (~1 km), and (3) that all previously documented cases of HF-induced seismicity in the United States have occurred in proximity ($\lesssim$2 km) from the associated stimulation.

To understand the significance of a $\Delta \mathrm{EQ}_{\mathrm{rate}}$ value, we follow the same validation approach of Skoumal, Ries, et al. (2018). We randomly swap origin times in our improved TexNet catalog to form 100 synthetic catalogs, and the $\Delta \mathrm{EQ}_{\mathrm{rate}}$ calculations are replicated for each synthetic case. With this approach, the relative regional seismicity and HF rates/locations are left unaltered and are used to inform us about the chances of spurious correlations between earthquakes and HF.

2.5. Quantifying the Amount of HF-Induced Seismicity

We introduce an alternative method to quantify the amount of HF-induced seismicity in the Delaware Basin, which is more quantifiable and accessible. If both WD- and HF-induced seismicity are in close spatial proximity to each other, the distinction between the two types of earthquakes can be difficult to identify by relying on changes in the earthquake rate. This limitation prevents HF-induced seismicity from being identified in central Oklahoma where high rates of WD-induced seismicity are located (Skoumal, Ries, et al., 2018). Large amounts of WD-induced seismicity also obscure the identification of HF-induced seismicity in the Delaware Basin, limiting the application of the $\Delta \mathrm{EQ}_{\mathrm{rate}}$ approach in high seismicity rate areas.

To improve the accuracy of our assessment of the total amount of HF-induced seismicity in the Basin, we use an alternative approach. We calculate the distance from every earthquake in our improved TexNet catalog to the nearest HF well that was being actively stimulated. We apply this same approach to the 100 synthetic earthquakes catalogs described previously. If HF-induced earthquakes are prevalent in a region, we would expect an increased number of earthquakes in close proximity to actively stimulating wells. On the contrary, if there are few or no HF-induced earthquakes, we would expect that the proximity between HF wells and earthquakes to fall near the 95% confidence bounds determined by the randomized trials. This simple approach allows us to approximate the prevalence of HF-induced seismicity in a region without relying on changes in earthquake rates that cannot isolate individual cases.

3. Results and Discussion

3.1. Improved Catalogs

Regional template matching applied to the 126 ANSS catalog earthquakes detects an additional 2,002 events (Figure 3c). Only 30 earthquakes (~1.5% of the catalog) are identified during 2009–2014 with the seismicity rate beginning to increase around 2015. Over half of the detected earthquakes occurred in 2018. However, as the regional ANSS catalog has a relatively high Mc ~2.9 (Figure S1 in the supporting information), the improved regional catalog is only able characterize earthquakes similar in character to those limited number of cataloged earthquakes. Frohlich et al. (2019) identified 7,514 earthquakes in our study area during 2000–2017 using a 10 station seismic array and produced a catalog with a M_C ~1. They demonstrated that seismicity began in the Reeves County area in ~2009 with seismicity rate beginning to increase in our study region (Figure 1) in ~2011. The seismicity rate increase generally follows the increase in WD volumes. Of the 369 $M \geq 2.0$ earthquakes identified by Frohlich et al. (2019) in our study region during 2009–2017, the regional template matching catalog was only able to identify 130 of these events (~35%); the Frohlich et al. (2019) catalog does a superior job of characterizing of the early onset seismicity in the Delaware Basin than the regional template matched catalog generated using ANSS cataloged events. For seismicity represented in the ANSS catalog, template matching produces a comparable result to Frohlich et al.'s (2019) catalog (Figure S2).

Local template matching applied to the 3,712 TexNet catalog earthquakes results in the detection of 36,874 events (Figure 3d). While all of these earthquakes occurred within approximately a 2-year window, it provides us with a larger catalog of events to better inform our other seismological characterizations. Template matching applied to the TexNet catalog produces identifies a larger number of events than Frohlich et al.'s (2019) catalog (Figure S2). However, in the high-activity region near and south of Pecos, the Frohlich et al. (2019) catalog reports hundreds of seismic events per year during 2010–2014 that template matching using the regional catalog was unable to detect. While template matching can improve the number of detected earthquakes, this is an example of the approach being unable to detect seismicity with magnitudes $< M_C$ that have waveforms that are dissimilar from those of cataloged events.

Of the 36,874 events identified from template matching using the TexNet network, 2,122 of them are located in our NW study area. Using the 319 originally cataloged earthquakes in this area, template matching applied to the New Mexico stations identifies 1,751 earthquakes (Figure 3e), 330 of which are new detections that were missed from template matching using the TexNet stations. Regional template matching identifies an additional 42 unique earthquakes for a total catalog of 2,494 events in the NW subregion. While template matching does not allow us to exclude the potential occurrence of seismicity in a region, we may conclude that there was very little seismicity in 2016–2017 that resembles the waveforms of later cataloged earthquakes in the northwestern portion of our study area. Considering there are no ANSS cataloged earthquakes before 2017 in this area, we would expect any previous seismicity to be small-magnitude events.

At the end of our study period, the seismicity rate continues to increase in the Delaware Basin. An increase in seismicity rate does not guarantee that earthquake magnitudes will increase beyond the previous observed M_{max} (M_L 3.7; M_W 3.4), so we cannot reliably determine whether larger magnitude events should be expected. However, when a larger magnitude earthquake is induced, it generally scales with the log of the total number of induced earthquakes in the sequence (van der Elst et al., 2016). If seismicity continues and the frequency magnitude distribution is to remain a log-linear relationship (Figure S1), additional events with magnitudes $\approx M_{max}$ must occur. Based on the frequency magnitude distribution determined during the entire duration of our study window, if a M_W 4.0 earthquake were to occur, we would expect an event of this size to have a recurrence interval of ~2 years. We note that since the seismicity rate increases throughout our study window, this estimate of the recurrence interval for a hypothetical M 4 earthquake may actually be shorter (more frequent) in the future. Based on our improved catalog, there is an underrepresentation of M_W 3.0-3.4 earthquakes assuming that the earthquakes follow a log-linear, Guttenberg-Richter relationship. We conclude that if seismicity continues and there are no changes to industrial operations, the Delaware Basin will likely experience an increased number of $M_W > 3$ earthquakes in the future with the ongoing potential for seismicity > M_W 3.4.

3.2. Examples of HF-Induced Seismicity

With the exception of some potential cases in northern Texas (Walter et al., 2018), no HF-induced seismicity has been previously identified in Texas. However, 274 cases of HF-induced seismicity were identified during 2010–2016 in Oklahoma (Skoumal, Ries, et al., 2018).

To maintain consistency with previous work identifying HF-induced seismicity in Oklahoma (Skoumal, Ries, et al., 2018), we set a threshold of $\Delta EQ_{rate} > 10$ and manually inspect all 28 wells that exceed this threshold (Figure 2). This threshold is above the 2σ bounds produced by the synthetic catalogs, so we have reasonable confidence that these are not spurious correlations (Figures 4a and 4b). Additionally, similar to previous work in Oklahoma, the 28 HF wells flagged tend to be located away from WD wells. The 28 HF wells with $\Delta EQ_{rate} > 10$ are associated with 1,191 earthquakes with $M \leq 2.8$ during the reported stimulation window. This represents ~3.2% of earthquakes in our improved catalog.

We see a correlation between the likelihood of HF-induced seismicity and proximity to basement (Figures 4c and 4d). The proximity of HF stimulations to critically stressed faults was previously suggested to be the primary factor controlling the likelihood of HF-induced seismicity (Skoumal, Brudzinski, & Currie, 2018). It is not possible to identify all critically stressed faults in a region, so the proximity to the Precambrian basement was used as a proxy. This assumption is well suited for many basins in the CEUS because the vast majority of induced earthquakes (and their associated seismogenic faults) is located in the basement. Contrary to this, in the Delaware Basin the majority of the industry operations are located where the sedimentary cover is thickest (~6–7 km), and many of the earthquake hypocenters are likely in the sedimentary rock. As a result, using the basement as a proxy for the seismogenic fault locations in the Delaware basin is not ideal. However, while most of the HF is ~3 km above the Precambrian basement (Figure 4c), we still do observe a much higher association between HF wells and earthquakes where HF stimulations are in close proximity to the basement (Figure 4d). While the high seismicity rates in areas of thick sedimentary cover obscure the identification of HF-induced seismicity, wells stimulated in proximity to the basement still have high associations (>20%) with induced seismicity.

Cases of HF-induced seismicity tend to spatially cluster (Skoumal et al., 2016; Skoumal, Ries, et al., 2018). A prominent example of this in the Delaware Basin is shown in Figure 5. Here, 32 unconventional wells stimulated the deeper (~3.6 km) Woodford Shale and three wells stimulated the shallower (~2.1 km) Bone Spring formation during the time period of our improved TexNet catalog. Of the 35 stimulated laterals, 19 (~54%) were associated with earthquakes, with 17 associated cases in the Woodford and two cases in the Bone Spring formations.

Nearly all (>99%) identified earthquakes in this area occur during hydraulic stimulations; the remaining earthquakes occur within 48 hr following a stimulation. With over half of the HF wells associated with earthquakes, this is among the highest occurrence rates of HF-induced seismicity in the United States, similar to the rate observed in Coal County, Oklahoma (~56%; Skoumal, Ries, et al., 2018). As shown in Figure 5, most of the cataloged earthquakes that were used as templates matched with events that occurred during the stimulations of multiple well laterals. Because of this waveform similarity, stimulations at different laterals likely induced earthquakes along similar fault(s) in close proximity to one another. With the exception of a few earthquakes, the cataloged events are < 2 km from the associated stimulated well. The TexNet reported absolute horizontal uncertainties for the earthquakes in this area are ~1.0 ($\pm$0.7) km. Considering these locations and their uncertainties, these observations are consistent with reported cases of HF-induced seismicity in the United States that are within ~1–2 km from stimulated wells (e.g., Skoumal et al., 2015b).

3.3. Quantifying the Amount of HF-Induced Seismicity

Our estimate of the amount of HF-induced seismicity based on the proximity to stimulating wells results in a slightly larger number of associated earthquakes when compared to using flagged wells that had

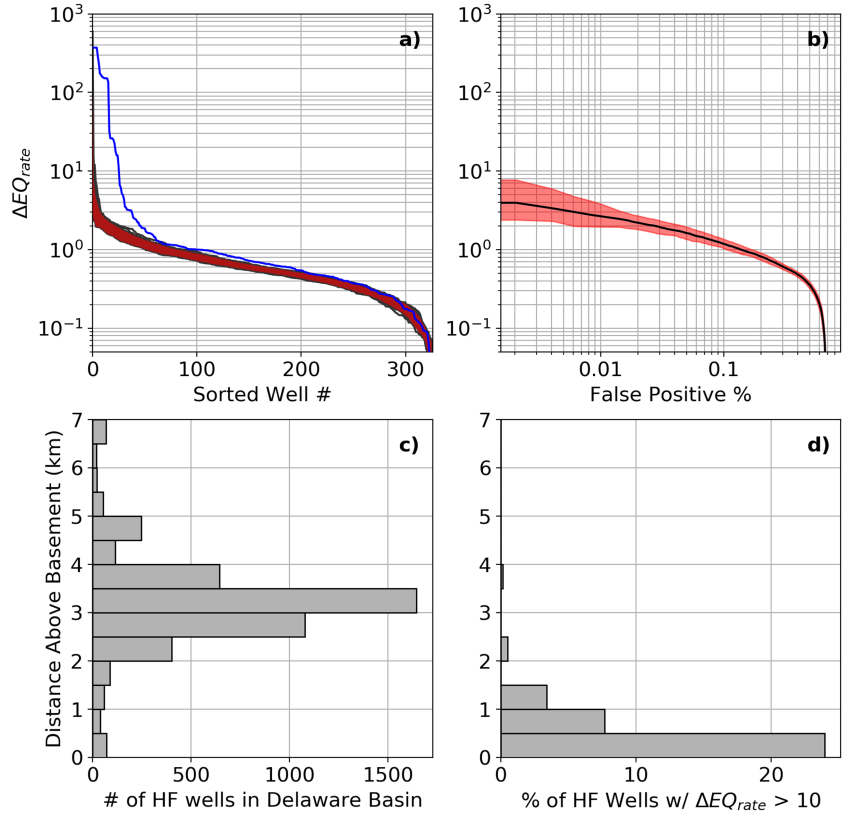

Figure 4. (a) ΔEQ_{rate} results for the hydraulic fracturing (HF) wells that had ≥5 earthquakes ≤7 km from the well using the improved TexNet earthquake catalog (blue line) compared against the results from 100 synthetic earthquake catalogs (black lines) and the 2σ range (red shading). Results are sorted by their ΔEQ_{rate}value. (b) The average probability (black line) and 2σ range (red shading) for the synthetic catalogs to produce a false positive correlation for a given ΔEQ_{rate} value. (c) Histogram of HF well proximity to the Precambrian basement. (d) Percentage of HF wells associated with earthquakes vs. proximity to basement.

$\Delta EQ_{rate} > 10$. A total of 1,850 earthquakes (~5.0% of catalog) are preferentially located near actively stimulating HF wells (Figure 6). As this HF-earthquake proximity method is not solely dependent on large changes in earthquake rates like the ΔEQ_{rate} method, a larger number of HF associated events is expected. These associated earthquakes are all located between ~0 and 5 km from active HF wells. From these results (Figure 6b), there was an ~30% chance that any earthquake within 5 km of an actively stimulated well is associated with HF (Figure 6c). We note that earthquakes induced more than 5 km from a hydraulic stimulation are unlikely, as HF-induced seismicity has yet to be confidently identified more than ~2 km from a stimulation. Rather, we suggest that the 5 km distance is a matter of both earthquake location uncertainties and our approximation that the stimulation was located at the well pad instead of true stimulation location in the horizontally drilled well. As stated previously in the ΔEQ_{rate} methodology, we think that it is possible that reported epicenters of HF-induced seismicity could be located as far as ~7 km from the surface pad in the Delaware Basin using conservative assumptions.

3.4. Wastewater Disposal-Induced Seismicity

In conventional oil plays, produced water can be reinjected back into the same formation, referred to as "waterflooding" rather than "WD." Waterflooding in conventional oil plays is used largely as a means to maintain reservoir pressure and/or to migrate hydrocarbons laterally toward an extraction well. In low permeability, unconventional oil plays, large volumes of produced water are often needed to be disposed into a different reservoir. With the rapid rise of unconventional wells in the Delaware Basin, particularly those targeting the Bone Spring and Wolfcamp formations, the amount of produced wastewater and the HF-related wastewater disposed of into separate reservoirs greatly increased (Figure 3a). This increase in hydrocarbon production and the resulting increase of WD volumes generally coincides with the increase of seismicity

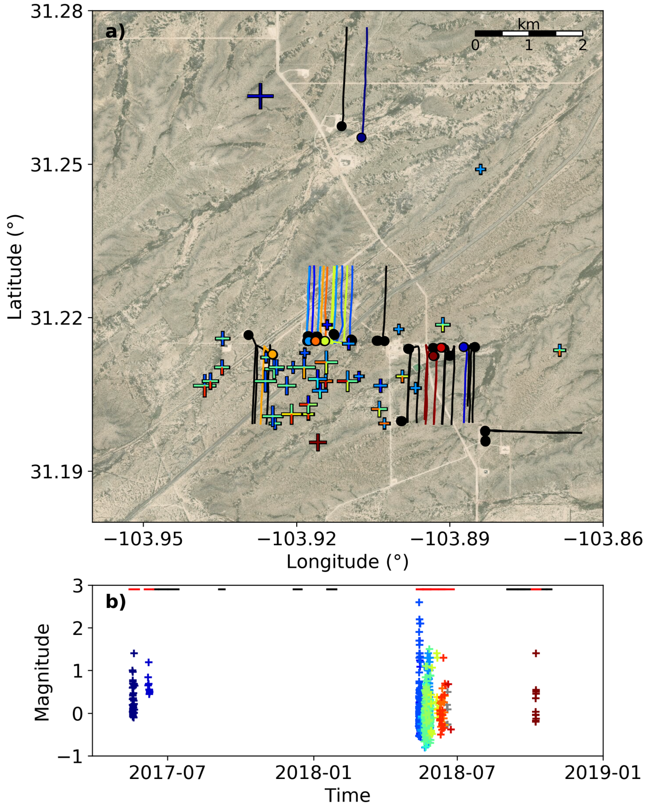

Figure 5. Examples of hydraulic fracturing (HF)-induced seismicity in the Delaware Basin. (a) Map of HF cases with earthquakes (crosses), well pads (circles), and horizontal well laterals (lines). Colored wells are associated with induced earthquakes. Earthquake symbols are sized by the number of detected events (between 1 and 51 earthquakes) that the respective template event identified. (b) Time series of earthquakes (crosses) and times of HF stimulations (bars) that are shown in (a). Colors of earthquakes represent the relative timing of induced sequences, consistent with colors in (a). TexNet reported absolute horizontal uncertainties for earthquakes in this area are ~1.0 (±0.7) km.

observed in the Basin (Figure 3c). Excluding the earthquakes induced by HF (~5% of the catalog; described previously) and those we are confident that are induced by far-field effects caused by WD (~3% of the catalog; described later), >95% of the remaining cataloged earthquakes occurred within 10 km of an active WD well.

The majority of WD wells in the Delaware Basin injected into the Delaware Mountain Group, composed of the Brushy Canyon, Cherry Canyon, and Bell Canyon formations. This Group is up to ~1.3 km thick and is composed of sandstone, siltstone, and limestone (Dutton et al., 2004). The WD wells injecting into these formations are shallower than the numerous HF wells targeting the Bone Spring and Wolfcamp formations (~2–3 km below sea level; Figures 7a and 7b). Although only a small number of WD wells in our study window inject into the deeper Devonian, Silurian, and Ordovician rocks, some of these wells have large injection rates, in excess of 10^6 bbl/month. In Oklahoma, WD into the basal Arbuckle Group is largely thought to be the cause of the induced earthquakes that have predominantly occurred a few kilometers below the Precambrian basement interface (e.g., Keranen et al., 2014). In the Delaware Basin, most of the TexNet cataloged earthquakes have reported hypocentral depths that also are a few kilometers below the WD wells (Figure 7). While the presence of induced earthquakes a few kilometers below the injection horizon in the Delaware Basin may appear to be consistent with previous observations in Oklahoma, the geology, earthquake locations, earthquake faulting mechanisms, and stress state must first be considered before drawing parallels.

The Arbuckle Group in Oklahoma is thought to be hydraulically connected to the Precambrian basement (e.g., Walsh & Zoback, 2015), while the Delaware Basin has multiple shale layers that impede such a simple vertical hydraulic connection. Additionally, hypocenter uncertainties in the Delaware Basin must be considered. The TexNet catalog has a reported median vertical uncertainty of 1.7 km, so many of these hypocentral depths may be shifted a couple kilometers vertically. The TexNet earthquake locations are based on a 1-D velocity developed for the Delaware Basin (Savvaidis et al., 2019), but a 3-D velocity model of the Delaware Basin is currently in development (Rathje et al., 2018). Along with improved velocity models, the earthquake depths may become better constrained as more instruments are deployed in the area.

With poorly constrained focal depths, it is challenging to determine the physical mechanism(s) responsible for seismicity in the Delaware Basin. This is partly because hydrocarbon production and WD are spatiotemporally similar (e.g., Figure S3), making it difficult to isolate their individual contributions. If the earthquake hypocentral depths are near the Delaware Mountain group, pore pressures and poroelastic effects within the reservoir could be more confidently associated with WD. Assuming hydraulic diffusivity is not reversed by elastic compliance, the presence of high-permeability conduits from fault damage-zones may also promote vertical diffusion of pore pressures to the lower formations. This could serve as a plausible source of high-permeability pathways for fluid diffusion. On the contrary, if the earthquake hypocentral depths are predominately below the interbedded shales and no such conduits exist, poroelastic effects due to production could explain why earthquakes occurred even without a direct hydraulic connection, albeit promoting failure on predominately normal or reverse faults (Chang & Segall, 2016). More than one third of the focal mechanisms from TexNet are reported as strike-slip, and while many mechanisms have large azimuthal gaps, these mechanisms are generally consistent with the normal and strike-slip faulting environment suggested by stress measurements (Snee & Zoback, 2018). If strike-slip mechanisms are prevalent in the Delaware Basin, hydrocarbon production is unlikely to be the primary cause of these earthquakes.

10.1029/2019JB018558

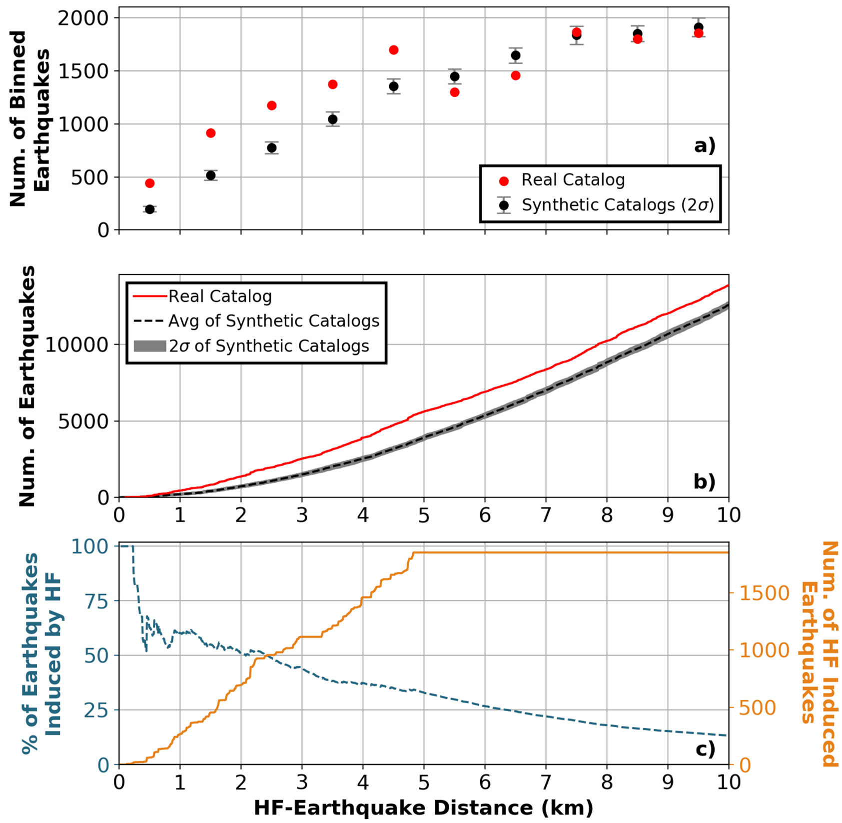

Figure 6. Distance-based associations between earthquakes and hydraulic fracturing (HF) wells. Distances between earthquakes and the closest actively stimulated well in (a) 1-km bins and (b) in continuous form for the real catalog (red) and synthetic catalogs (black, with 2σ error regions). (c) Earthquakes associated with HF—the difference between the observed and synthetic catalogs in (b)—expressed as a percentage of events (dashed line) and total number of events (solid line).

To evaluate the potential influence of production contributing to the seismicity, we performed a simplified estimate of the stress change that would result from the production of fluids. During 2007–2017, ~1.1×10^9 barrels (~1.7×10^8 m^3) of fluid was disposed of in Reeves county (an area of 6,843 km^2), where the seismicity occurred (Figure S3). We conservatively assume that (1) all WD fluid was originally produced water, (2) the

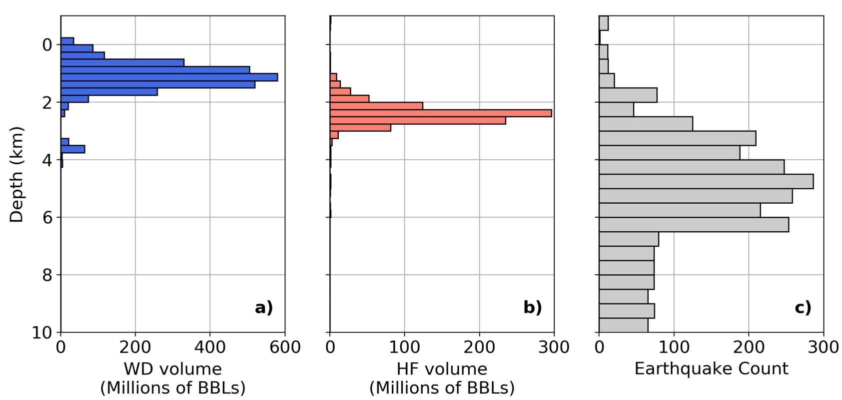

Figure 7. Depths (histograms) of (a) wastewater disposal (WD) volumes during 2007–2017, (b) hydraulic fracturing (HF) stimulation volumes during 2011–2018, and (c) TexNet catalog earthquakes in the Delaware Basin. All depths are relative to sea level. WD volumes are assumed to be injected at the maximum permitted injection depth, and only wells with reported permit depths are considered. Only TexNet earthquakes with hypocentral depths < 10 km and vertical uncertainties < 2 km are shown.

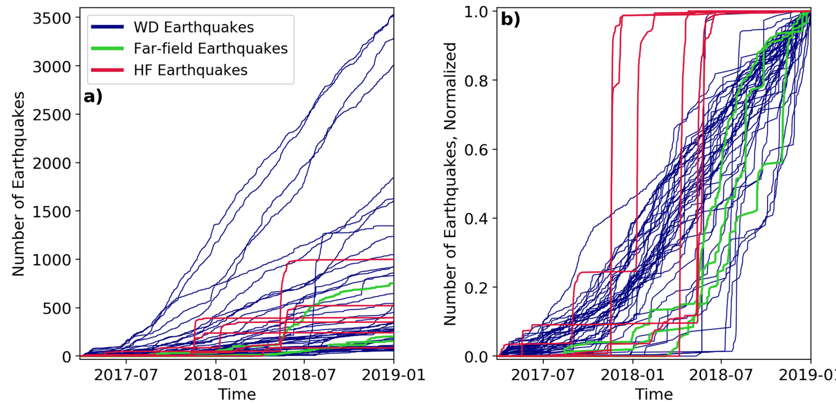

Figure 8. Cumulative number of earthquakes in our study identified over time divided into 0.1° geographical bins. The lines are colored by whether the bins are dominated by seismicity induced by wastewater disposal (WD; blue), far-field effects (green), or hydraulic fracturing (HF; red).

WD fluid does not counteract the mass loss of the produced water, (3) there was a 1:1 ratio of produced water: hydrocarbons such that a total of ~2.2 billion barrels (~3.4×10^8 m^3) of fluid was extracted, and (4) pressure decline in the reservoir is uniform across the region. With those assumptions there would be the equivalent of ~5.1-cm fluid head decline associated with withdrawal, equivalent to an ~0.5-kPa hydrostatic pressure change. Even given our conservative assumptions, this estimated pressure change is roughly 2 orders of magnitude smaller than stress changes observed for natural earthquake triggering (e.g., Gomberg & Johnson, 2005), about a factor of 3 smaller than the average stress changes associated with either atmospheric pressure loading or solid earth tides (e.g., Barbour et al., 2019), with only scant evidence of tide-triggered seismicity (e.g., Cochran et al., 2004; Vidale et al., 1998). A similar methodology that produced a larger estimated stress change was previously used to argue that seismicity in the Raton Basin was induced by WD rather than production (Rubinstein et al., 2014). To test this further, we evaluate the influence of production on the seismicity by computing poroelastic stresses in the rock assuming an axisymmetric reservoir where pore pressure changes due to production vary with radial distance and depth alone (Segall, 1992). These simulations (Figure S5) indicate regions where stress concentrations develop—most significantly at the edges of the hypothetical reservoir—but the magnitude of changes to the maximum shear stress and mean stress fields at seismogenic depths are small fractions of the assumed pressure change in the reservoir. Hence, it seems that production-related effects are not the primary cause for this seismicity.

The earthquakes demonstrated swarm-like behavior, disparate from mainshock-aftershock or "isolated" earthquake patterns that commonly occur for natural seismicity throughout the CEUS (Figure 8). The coefficient of variation (Cv) of interevent earthquake times (T; Kagan & Jackson, 1991), defined as the ratio of the standard deviation of T to the average T, is a measure of whether earthquakes are quasi-periodic (Cv < 1), Poissonian (Cv = 1), or clustered (Cv > 1). Induced seismicity in southern Kansas has a Cv between 1 and 8 (Cochran et al., 2018). In Oklahoma, ~90% of cases in Oklahoma also have a Cv between 1and 8, although areas with HF-induced seismicity or relatively large (M > 4) magnitude earthquakes have a Cv as large as ~20 (Skoumal, Brudzinski, et al., 2019). Similar to Skoumal, Brudzinski, et al., (2019), we group seismicity in 0.1° × 0.1° geographical bins and we determine whether seismicity is predominately induced by WD or HF. We find that the WD and HF earthquakes have a Cv of 2.9 (±2.1) and 9.8 (±1.7), respectively, which are similar to values reported previously in Kansas and Oklahoma (Cochran et al., 2018; Skoumal, Brudzinski, et al., 2019). These high Cv results imply that earthquakes are strongly clustered, as visible in Figure 8.

3.5. Far-Field Effects of WD

The seismicity in the NW study area largely began in mid-August 2017 with only a handful of earthquakes identified in the previous few months (Figure 9). No earthquakes in this area were identified in the ANSS catalog before 2017. While it is possible that there may be other small, uncatalogued earthquakes in the NW area before mid-2017, we do not find any earthquakes similar to those reported in the ANSS or TexNet catalogs from template matching. As these earthquakes occurred after the TexNet stations were

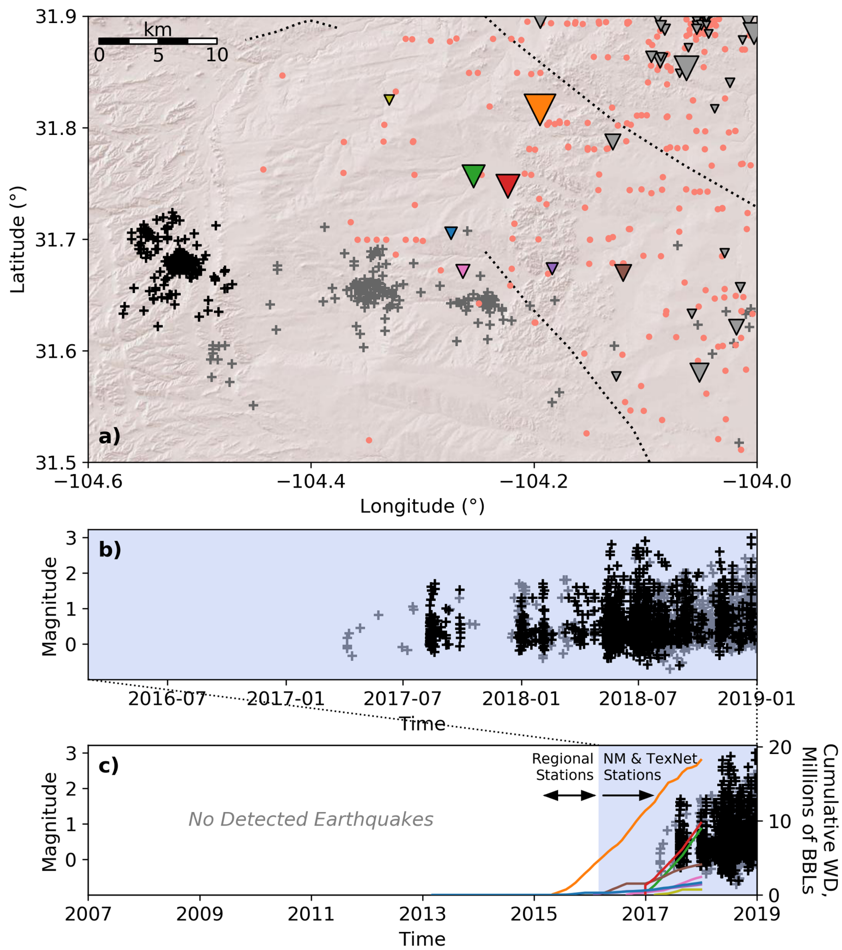

Figure 9. (a) Map of earthquakes (crosses), wastewater disposal (WD) wells (triangles), and hydraulic fracturing (HF) wells (circles). Colored WD wells represent wells <40 km from the western cluster, and the size of the triangles represents the relative cumulative injection volume at the WD wells. The dashed lines represent previously mapped faults. The black crosses represent earthquakes in the westernmost cluster, with the gray crosses representing all other earthquakes in the area. The black crosses indicate those in the westernmost cluster. (b) Magnitude of earthquakes in this area over time. (c) Cumulative WD volumes (lines) during 2007–2017 compared against the detected earthquakes (crosses). The WD line colors are consistent with (a).

deployed, the hypocenters of the cataloged seismicity are reasonably constrained; the reported horizontal uncertainties are ~0.8 (±0.4) km. The cataloged earthquakes in the NW area occurred in three spatial clusters. The westernmost cluster of earthquakes is the most intriguing as it was located the furthest (~25 km) from the nearest WD well. While the nearest WD well was a relatively moderate-rate disposal well (~10^5 barrels/month), there are WD wells in this area that exceed 10^6 barrels/month ~30 km away, a rate in the top 1% of injection rate wells in the Delaware Basin. These high-rate wells inject into the Silurian (~4.5-km depth), while the all other WD wells within ~40 km of the west seismicity cluster injected into the shallower Delaware Mountain Group (~1-km depth).

In Oklahoma, the 2016 M_W 5.1 Fairview earthquake sequence may have been induced by poroelastic effects from WD wells that were >40 km away from the earthquakes (Goebel et al., 2017; Yeck et al., 2016). However, the history of WD within 10 km of the earthquakes (McGarr & Barbour, 2018) challenges whether far-field effects are principally responsible. Because all of the WD in the NW study area in the Delaware Basin is further than ~25 km away from the seismicity, we have the opportunity to analyze far-field effects without the uncertainties of injection close to the earthquake sources. Additionally, we can rule out HF as the source of these induced earthquakes because there are no reported HF wells within 10 km of the NW seismicity, and the sequence is atypical of the short-lived HF-induced cases observed elsewhere.

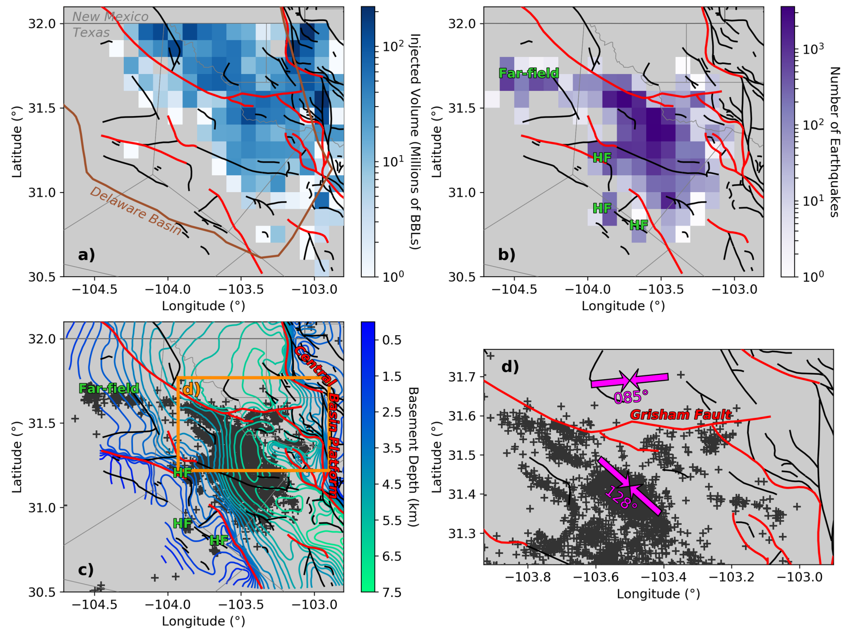

Figure 10. (a) Total injection volumes during 2007–2018 in 0.1 deg geographical bins. (b) Number of earthquakes in our improved TexNet catalog during 2017–2018. Areas dominated by hydraulic fracturing (HF) or far-field-induced seismicity are labeled. (c) Contours of basement depth (relative to sea level) and earthquakes (crosses). (d) Closer view of the Grisham fault, SHmax orientations (arrows), and earthquakes (crosses). The black and red lines are mapped faults (Ruppel et al., 2008), with the red lines hypothesized to be low-permeability flow barriers.

Based on our observations and numerical simulations of injection, we suggest that these earthquakes are most likely induced by far-field effects due to WD wells. As this sequence is a long-lived, productive earthquake swarm with a seismicity rate that continues to increase, it is aberrant from natural seismicity in the CEUS. While no natural earthquakes resembling this NW sequence have been observed elsewhere in the Mid-Continental United States, the rapid increase in seismicity rate does resemble the productive, swarm-like nature of induced seismicity Oklahoma. The onset of the NW cluster in 2017 and the continual increase in the seismicity rate since then is similar to the seismicity rate increases observed elsewhere in the Delaware Basin, supporting the conclusion that these NW earthquakes are also induced. Based on our numerical simulations, the hydraulic diffusivity would likely have to be in excess of 1 m^2/s if the pore pressure increases from these WD wells are responsible. If our catalog is missing earthquakes earlier in the sequence, the requisite diffusivity would be even higher. This analysis does not preclude the possibility that earthquake migration is a result of rapid pressure diffusion along a narrow high-permeability pathway with an east-west orientation, of the type that helps explain rapid seismicity migration in otherwise low-permeability crystalline rock (e.g., Hsieh & Bredehoeft, 1981). Such an explanation would suggest a major role of fracture zones and/or fault damage zones, implying that fluid pressures may be compartmentalized.

3.6. Impact of Basin Structure on Industry Operations and Earthquakes

Hydrocarbon production and WD are occurring throughout the Delaware Basin in Texas (Figures 10a and S4), but cataloged earthquakes have largely occurred in the southern portion of this Basin (Figure 10b). Understanding the occurrence (and lack) of induced earthquakes is a crucial component of addressing the hazard of induced seismicity. Production and WD depths are similar across the Grisham fault, and we are not aware of any differences in industry operations that would be consistent with a lack of seismicity north of the Grisham fault.

Geologic structures can play an important role in influencing induced seismicity. In Oklahoma, the Nemaha fault is thought to be a low-permeability barrier that impedes horizontal fluid diffusion, altering regional seismicity rates (e.g., Langenbruch et al., 2018). The fault is also associated with S_{Hmax} rotation and an area of relative seismic quiescence (Skoumal, Kaven, & Walter, 2019). In the Delaware Basin, the western edge of the Central Basin Platform (Figure 10c) and the Grisham fault to the north (Figure 10d) delineate the extent of seismicity. As the Central Basin Platform is a tectonically uplifted basement block (Figure 10c), horizontal fluid migration would likely be inhibited. Strong, systematic changes in the S_{Hmax} direction are observed across the Grisham fault (Forand et al., 2017; Snee & Zoback, 2018; Figure 10d), which suggests that perhaps the magnitude of crustal stresses impacts the occurrence of seismicity. Absolute stress measurements and better constraints on the stress rotation in the vicinity of the Grisham fault would aid our understanding of the induced earthquakes.

Could a lack of critically stressed, optimally oriented faults in the area north of the Grisham fault potentially be the reason for the relative seismic quiescence? Rubinstein et al. (2018) and Peterie et al. (2018) suggest the large (up to 10 km) separation between earthquake clusters in Kansas is due to the absence of critically stressed, optimally oriented faults. North of the Grisham fault, however, this aseismic region is many times larger than what was observed in Kansas; rather than there being spatial gaps between seismicity, the region is devoid of cataloged earthquakes. We do not think that a total absence of seismogenic faults over such a large geographical area is the most likely explanation. Considering that small, critically stressed faults were found to be ubiquitous in Oklahoma (Skoumal, Kaven, et al., 2019) and that seismicity in the southern Delaware Basin is mostly occurring along previously unmapped faults, it is reasonable to assume that there would be at least a small number of potentially seismogenic faults north of the Grisham fault.

Alternatively, considering the spatial correlation between seismicity and major structures, we may assume that major structures act as low-permeability barriers. Hypothetically, these structures would compartmentalize injected fluids, resulting in elevated reservoir pressures in the southern portion of the Basin, and more general diffusion toward the north into New Mexico. Presently, we cannot test this observationally as there are no publicly available pore pressure data, but poroelastic modeling that includes three-dimensional reservoir details may be able to provide meaningful insight into the role these hypothesized low-permeability barriers may have in controlling the distribution of pore pressure and induced stresses in the Basin. Potential variations in the overpressurization of geologic formations and the impact this has on faults should be considered. One expectation would be that initial reservoir pressures would vary across the Grisham fault; higher reservoir pressures in formations south of the fault could help explain the seismic quiescence.

4. Conclusions

We used three template matching catalogs to characterize the recent seismicity in the Delaware Basin in western Texas during 2009–2018. The improved catalogs contain ~37,000 unique earthquakes with $M_W \leq 3.4$. Nearly all of the seismicity is spatiotemporally correlated with industry operations and is most likely induced by these activities. The majority of these earthquakes are associated with WD, but at least ~5% of the seismicity appears to be associated with HF stimulations. Using the HF-earthquake proximity method, we found that there was an ~30% chance that any earthquake within 5 km of an actively stimulated well was associated with HF. Earthquakes in the northwest portion of our study area are best described as induced by far-field (>25 km) effects of WD, with known geologic structures (e.g., Central Platform, Grisham Fault) influencing the location of the seismicity. The seismicity rate increased throughout the duration of our study window. If industry operations continue unaltered, both the seismicity rate and number of M > 3 earthquakes may continue to increase in the future.

Acknowledgments
All seismic data were obtained through the Incorporated Research Institutions for Seismology Data Management Center (www.iris.edu; last accessed March 2019). The IM (http://www.fdsn.org/networks/detail/IM), SC (http://www.fdsn.org/networks/detail/SC), TA (https://doi.org/10.7914/SN/TA), TX (https://doi.org/10.7914/SN/TX), and US (https://doi.org/10.7914/SN/US) seismic networks were utilized in this study. Well data were retrieved from FracFocus (https://fracfocus.org; last accessed March 2019) and the Texas Railroad Commission (rrc.texas.gov; last accessed March 2019). Earthquake catalogs were obtained from the ANSS (https://www.usgs.gov/natural-hazards/earthquake-hazards/earthquakes; last accessed October 2019), and TexNet (http://coastal.beg.utexas.edu/texnetcatalog; last accessed March 2019). Basement depth contours and mapped faults were obtained from the Permian Basin Geologic Synthesis Project (http://www.beg.utexas.edu/resprog/permianbasin/gis.htm; last accessed March 2019). This work benefited from discussions with Justin Rubinstein, Elizabeth Cochran, Jeff Nunn, and William Ellsworth. Elizabeth Cochran, Cliff Frohlich, Art McGarr, and Justin Rubinstein provided helpful peer reviews that improved the manuscript. The authors declare that they have no competing interests. Any use of trade, firm, or product names is for descriptive purposes only and does not imply endorsement by the U.S. Government.

References

Barbour, A. J., Xue, L., Roeloffs, E., & Rubinstein, J. L. (2019). Leakage and increasing fluid pressure detected in Oklahoma's wastewater disposal reservoir. *Journal of Geophysical Research: Solid Earth: Solid Earth*, *124*, 2896–2919. https://doi.org/10.1029/2019JB017327

Chang, K. W., & Segall, P. (2016). Seismicity on basement faults induced by simultaneous fluid injection–extraction. *Pure and Applied Geophysics*, *173*(8), 2621–2636.

Cochran, E. S., Ross, Z. E., Harrington, R. M., Dougherty, S. L., & Rubinstein, J. L. (2018). Induced earthquake families reveal distinctive evolutionary patterns near disposal wells. *Journal of Geophysical Research: Solid Earth: Solid Earth*, *123*, 8045–8055. https://doi.org/10.1029/2018JB016270

Cochran, E. S., Vidale, J. E., & Tanaka, S. (2004). Earth tides can trigger shallow thrust fault earthquakes. *Science*, *306*(5699), 1164–1166. https://doi.org/10.1126/science.1103961

Davis, S. D., & Pennington, W. D. (1989). Induced seismic deformation in the Cogdell oil field of west Texas. *Bulletin of the Seismological Society of America*, *79*, 1477–1495.

Doser, D. I., Baker, M. R., & Mason, D. B. (1991). Seismicity in the War-Wink gas field, Delaware Basin, west Texas, and its relationship to petroleum production. *Bulletin of the Seismological Society of America*, *81*(3), 971–986.

Dutton, S. P., Kim, E. M., Broadhead, R. F., Breton, C. L., Raatz, W. D., Ruppel, S. C., & Kerans, Charles (2004). Play analysis and digital portfolio of major oil reservoirs in the Permian Basin: application and transfer of advanced geological and engineering technologies for incremental production opportunities: The University of Texas at Austin, Bureau of Economic Geology, and New Mexico Bureau of Geology and Mineral Resources, New Mexico Institute of Mining and Technology, annual report prepared for U.S. Department of Energy, under contract no. DE-FC26-02NT15131.

Ellsworth, W. L. (2013). Injection-induced earthquakes. *Science*, *341*(6142), 1225942. https://doi.org/10.1126/science.1225942

Forand, D., V. Heesakkers, & K. Schwartz (2017). Constraints on natural fracture and in-situ stress trends of unconventional reservoirs in the Permian Basin, USA. Unconventional Resources Technology Conference. doi: 10.15530/URTEC-2017-2669208

Frohlich, C., DeShon, H., Stump, B., Hayward, C., Hornbach, M., & Walter, J. I. (2016). A historical review of induced earthquakes in Texas. *Seismological Research Letters*, *87*(4), 1022–1038.

Frohlich, C., Ellsworth, W. L., Brown, W. A., Brunt, M., Luetgert, J. H., MacDonald, T., & Walter, S. (2014). The 17 May 2012 M 4.8 earthquake near Timpson, east Texas: An event possibly triggered by fluid injection, J. Geophys. Res. *Solid Earth*, *119*, 581–593. https://doi.org/10.1002/2013JB010755

Frohlich, C., Hayward, C., Rosenblit, J., Aiken, C., Hennings, P., Savvaidis, A., et al. (2019). Onset and cause of increased seismic activity near Pecos, West Texas, USA from observations at the Lajitas TXAR Seismic Array. *Journal of Geophysical Research: Solid Earth: Solid Earth.*. https://doi.org/10.1029/2019JB017737

Frohlich, C., Hayward, C., Stump, B., & Potter, E. (2011). The Dallas–Fort Worth earthquake sequence: October 2008 through May 2009. *Bulletin of the Seismological Society of America*, *101*(1), 327–340. https://doi.org/10.1785/0120100131

Gan, W., & Frohlich, C. (2013). Gas injection may have triggered earthquakes in the Cogdell oil field, Texas. *Proceedings of the National Academy of Sciences*, *110*(47), 18,786–18,791. https://doi.org/10.1073/pnas.1311316110

Goebel, T. H. W., Weingarten, M., Chen, X., Haffener, J., & Brodsky, E. E. (2017). The 2016 Mw5. 1 Fairview, Oklahoma earthquakes: Evidence for long-range poroelastic triggering at > 40 km from fluid disposal wells. Earth Planet. *Science Letters*, *472*, 50–61. https://doi.org/10.1016/j.epsl.2017.05.011

Gomberg, J., & Johnson, P. A. (2005). Dynamic triggering of earthquakes. *Nature*, *437*(4060), 830. https://doi.org/10.1038/437830a

Herzog, M. (2014). *Investigation of possible induced seismicity due to wastewater disposal in the Delaware Basin*. Dagger Draw Field, New Mexico-Texas, USA: Honors thesis, University of Colorado.

Hornbach, M. J., DeShon, H. R., Ellsworth, W. L., Stump, B. W., Hayward, C., Frohlich, C., et al. (2015). Causal factors for seismicity near Azle, Texas. *Nature Communications*, *6*(1), 1–11. https://doi.org/10.1038/ncomms7728

Hsieh, P. A., & Bredehoeft, J. D. (1981). A reservoir analysis of the Denver earthquakes: A case of induced seismicity. *Journal of Geophysical Research*, *86*(B2), 903–920. https://doi.org/10.1029/JB086iB02p00903

Kagan, Y. Y., & Jackson, D. D. (1991). Long-term earthquake clustering. *Geophysical Journal International*, *104*(1), 117–134. https://doi.org/10.1111/j.1365-246X.1991.tb02498.x

Kaven, J. O., Hickman, S. H., McGarr, A. F., & Ellsworth, W. L. (2015). Surface monitoring of microseismicity at the Decatur, Illinois, CO_2 sequestration demonstration site. *Seismological Research Letters*, *86*(4), 1096–1101. https://doi.org/10.1785/0220150062

Keranen, K. M., Weingarten, M., Abers, G. A., Bekins, B. A., & Ge, S. (2014). Sharp increase in central Oklahoma seismicity since 2008 induced by massive wastewater injection. *Science*, *345*(6195), 448–451. https://doi.org/10.1126/science.1255802

Langenbruch, C., Weingarten, M., & Zoback, M. D. (2018). Physics-based forecasting of man-made earthquake hazards in Oklahoma and Kansas. *Nature Communications*, *9*(1), 3946. https://doi.org/10.1038/s41467-018-06167-4

McGarr, A., & Barbour, A. J. (2018). Injection-induced moment release can also be aseismic. *Geophysical Research Letters*, *45*, 5344–5351. https://doi.org/10.1029/2018GL078422

Peterie, S. L., Miller, R. D., Intfen, J. W., & Gonzales, J. B. (2018). Earthquakes in Kansas induced by extremely far-field pressure diffusion. *Geophysical Research Letters*, *45*(3), 1395–1401.

Pursley, J., Bilek, S., & Ruhl, C. J. (2013). Earthquake catalogs for New Mexico and bordering areas: 2005-2009. *New Mexico Geology*, *35*(1), 3–12.

Rathje, E., P. Hennings, A. Savvaidis, & M. Young (2018). 2018 biennial report on seismic monitoring and research in Texas. https://www.beg.utexas.edu/texnet-cisr/reports

Rubinstein, J. L., Ellsworth, W. L., & Dougherty, S. L. (2018). The 2013–2016 induced earthquakes in Harper and Sumner Counties, Southern Kansas, The 2013–2016 induced earthquakes in Harper and Sumner Counties. *Southern Kansas Bulletin of the Seismological Society of America*, *108*(2), 674–689.

Rubinstein, J. L., Ellsworth, W. L., McGarr, A., & Benz, H. M. (2014). The 2001–present induced earthquake sequence in the Raton Basin of northern New Mexico and southern Colorado. *Bulletin of the Seismological Society of America*, *104*(5), 2162–2181.

Rubinstein, J. L., & Mahani, A. B. (2015). Myths and facts on wastewater injection, hydraulic fracutring, enhanced oil recovery, and induced seismicity. *Seismological Research Letters*, *86*(4), 1060–1067. https://doi.org/10.1785/0220150067

Ruppel, S.C., R. Loucks, C. Kerans, R.H. Jones, H.S. Nance, C.L. Breton, et al. (2008). Integrated synthesis of the Permian Basin. http://www.beg.utexas.edu/resprog/permianbasin/integsynthesis.htm

Savvaidis, A., Young, B., Huang, G. C. D., & Lomax, A. (2019). TexNet: A statewide seismological network in Texas. *Seismological Research Letters*. https://doi.org/10.1785/0220180350

Schaff, D. P., & Richards, P. G. (2014). Improvements in magnitude precision, using the statistics of relative amplitudes measured by cross correlation. *Geophysical Journal International*, *197*(1), 335–350. https://doi.org/10.1093/gji/ggt433

Schaff, D. P., & Waldhauser, F. (2010). One magnitude unit reduction in detection threshold by cross correlation applied to Parkfield (California) and China seismicity. *Bulletin of the Seismological Society of America*, *100*(6), 3224–3238.

Segall, P. (1992). Induced stresses due to fluid extraction from axisymmetric reservoirs. *PAGEOPH*, *139*(3-4), 535–560. https://doi.org/10.1007/BF00879950

Skoumal, R. J., Brudzinski, M., & Currie, B. (2015a). Distinguishing induced seismicity from natural seismicity in Ohio using waveform template matching. *Journal of Geophysical Research*, *120*(9), 6284–6296. https://doi.org/10.1002/2015JB012265

Skoumal, R. J., Brudzinski, M., & Currie, B. (2015b). Earthquakes induced by hydraulic fracturing in Poland Township, Ohio. *Bulletin of the Seismological Society of America*, *105*(1), 189–197.

Skoumal, R. J., Brudzinski, M., & Currie, B. (2016). An efficient repeating signal detector to investigate earthquake swarms. *Journal of Geophysical Research*, *121*(8). https://doi.org/10.1002/2016JB012981

Skoumal, R. J., Brudzinski, M., & Currie, B. (2018). Proximity of Precambrian basement affects the likelihood of induced seismicity in the Appalachian, Illinois, and Williston Basins. *Geosphere*, *14*(3). https://doi.org/10.1130/GES01542.1

Skoumal, R. J., Brudzinski, M., Currie, B., & Levy, J. (2014). Optimizing multi-station earthquake template matching through re-examination of the Youngstown, Ohio, sequence. *Earth and Planetary Science Letters*, *405*, 274–280. https://doi.org/10.1016/j.epsl.2014.08.033

Skoumal, R. J., Brudzinski, M., Currie, B., & Ries, R. (2019). Temporal patterns of induced seismicity in Oklahoma revealed from multi-station template matching. *Journal of Seismology*, 1–15. https://doi.org/10.1007/s10950-019-09864-9

Skoumal, R. J., Kaven, J. O., & Walter, J. I. (2019). Characterizing seismogenic fault structures in oklahoma using a relocated template-matched catalog. *Seismological Research Letters*. https://doi.org/10.1785/0220190045

Skoumal, R. J., Ries, R., Brudzinski, M., Barbour, A., & Currie, B. (2018). Earthquakes induced by hydraulic fracturing are pervasive in Oklahoma. *Journal of Geophysical Research*, *123*, 10,918–10,935. https://doi.org/10.1029/2018JB016790

Snee, J.-E. L., & Zoback, M. (2018). State of stress in the Permian Basin, Texas and New Mexico: implications for induced seismicity. *The Leading Edge*, *37*(2), 127–134. https://doi.org/10.1190/tle37020127.1

van der Baan, M., & Calixto, F. J. (2017). Human-induced seismicity and large-scale hydrocarbon productions in the US and Canada. *Geochemistry, Geophysics, Geosystems*, *18*, 2467–2485. https://doi.org/10.1002/2017GC006915

Vidale, J. E., Agnew, D. C., Johnston, M. J. S., & Oppenheimer, D. H. (1998). Absence of earthquake correlation with Earth tides: An indication of high preseismic fault stress rate. *Journal of Geophysical Research*, *103*(B10), 24,567–24,572. https://doi.org/10.1029/98JB00594

Walsh, F. R., & Zoback, M. D. (2015). Oklahoma's recent earthquakes and saltwater disposal. *Science Advances*, *1*(5), e1500195. https://doi.org/10.1126/sciadv.1500195

Walter, J. I., Frohlich, C., & Borgfeldt, T. (2018). Natural and induced seismicity in the Texas and Oklahoma Panhandles. *Seismological Research Letters*, *89*(6), 2437–2446.

Wiemer, S., & Wyss, M. (2000). Minimum magnitude of completeness in earthquake catalogs: Examples from Alaska, the Western United States, and Japan. *Bulletin of the Seismological Society of America*, *90*(4), 859–869.

Yeck, W. L., Weingarten, M., Benz, H. M., McNamara, D. E., Bergman, E. A., Herrmann, R. B., et al. (2016). Far-field pressurization likely caused one of the largest injection induced earthquakes by reactivating a large preexisting basement fault structure. *Geophysical Research Letters*, *43*(19), 10–198.

Zhang, Y., Edel, S. S., Pepin, J., Person, M., Broadhead, R., Ortiz, J. P., et al. (2016). Exploring the potential linkages between oil-field brine reinjection, crystalline basement permeability, and triggered seismicity for the Dagger Draw Oil field, southeastern New Mexico, USA, using hydrologic modeling. *Geofluids*, *16*(5), 971–987. https://doi.org/10.1111/gfl.12199